Single-particle momentum distributions in sodium clusters: dependence on deformation

A. Rigo, M. Casas, and F. Garcias
Departament de Física, Universitat de les Illes Balears
E-07071 Palma de Mallorca, Spain

E. Moya de Guerra and P. Sarriguren
Instituto de Estructura de la Materia, C.S.I.C.
Serrano 123, E-28006 Madrid, Spain

Recibido el 16 de agosto de 1999; aceptado el 17 de septiembre de 1999

The main properties of deformed sodium clusters in momentum space have been analyzed in the framework of the selfconsistent Kohn-Sham formalism using a spheroidal jellium configuration. Deformation effects in r space have been compared with those in k space for both global and single-particle distributions. In momentum space, deformation has more effect in single-particle distributions and its behavior is a signature of the admixture of various l-waves in each deformed orbital.

Keywords: Atomic clusters; electronic structure

Mediante el formalismo de Kohn-Sham autoconsistente y usando una configuración de jellium esferoidal se han analizado las principales propiedades de los agregados de sodio deformados en el espacio de momentos. Los efectos de la deformación en el espacio r se han comparado con los correspondientes en el espacio k, tanto para la distribución global como para la de partícula simple. En el espacio de momentos, la deformación tiene un efecto mayor en las distribuciones de partícula simple y su comportamiento es una indicación de la mezcla de varias ondas l en cada orbital deformado.

Descriptores: Agregados atómicos; estructura electrónica

PACS: 71.24.+q; 61.46.+w; 36.40.-c; 31.15.Ew

1. Introduction

There are clear experimental evidences that metal clusters with partially filled electronic shells break spherical symmetry and become deformed [1, 2]. Deformation effects can be seen in the behavior of electron affinities, ionization potentials and in the double structure of the resonance peak of the photoabsortion spectra [3–5]. The energy density functional formalism has given reasonable predictions of many experimental properties for deformed sodium clusters in r space [6–9]. Predictions in k space have received less attention, even though electronic momentum distributions have been recently measured in other systems [10], like fullerenes [11] and noble gases [12], and provide valuable information for the correlation energy of the electron gas [13].

Recently, the global properties in momentum space for spherical and deformed Na clusters have been analyzed [14–16] and, in particular, the effect of the ionic background deformation in the overall momentum distribution [16] has been studied. Our previous work [15, 16] was based on the selfconsistent Kohn-Sham formalism with a spheroidal jellium configuration, a realistic manageable method to treat these complex systems.

In principle, the momentum distributions of the valence electrons in each individual shell could be mapped out by coincidence electron knock-out experiments, in a way similar to what is done in other microscopic systems [17]. It is therefore interesting to know how these individual momentum distributions may look like depending on the global shape of the cluster. With this view in mind we examine here the momentum distributions of the outermost shells in various sodium clusters following the same approximation as in our previous work.

2. Formalism

We assume that the main properties of the ground state of sodium clusters can be understood from the selfconsistent solution of the Kohn-Sham equations obtained from an energy density functional (Hartree atomic units have been used throughout the text),

$$\Big[-\frac{1}{2}\nabla^2 + \int \frac{n(\vec{r'})}{|\vec{r}-\vec{r'}|}\,d\vec{r'} + V_{xc}(n(\vec{r})) + v_{je}(\vec{r})\Big]\varphi_j(\vec{r}) = \varepsilon_j\varphi_j(\vec{r}). \quad (1)$$

In our results the exchange correlation potential $V_{xc}(n(\vec{r}))$ is taken in the local density approximation, and for simplicity we have used the Wigner approach for the correlation part. The ionic background $v_{je}(\vec{r})$ is modelled as in

Refs. 8 and 16 using an axially-symmetric jellium with constant volume. We have solved the Kohn-Sham equations in cylindrical coordinates. The ground state density $n(\vec{r})$ of Na clusters is determined by requiring that the ionic background deformation minimizes the total energy of the system. As shown in Ref. 16, an equivalent way is to search for the configuration that gives a null value of the quadrupole moment in k space.

The solution of the Kohn-Sham equations provides us the single-particle wave function for each j-orbital $\{\varphi_j(\rho, z)\}$, and the corresponding eigenenergies. Hence, the single-particle wave function in momentum space, $\tilde{\varphi}_j(k_\rho, k_z)$, is the Fourier transform of $\varphi_j(\rho, z)$.

The l angular momentum component for a single-particle orbital is obtained by expanding $\varphi_j(\rho, z)$ into eigenfunctions of a spherical harmonic-oscillator (HO) potential

$$|\varphi_j(\rho, z)e^{im\phi}\rangle = \sum_{nl} C_{nl}|u_{nl}(r)Y_{lm}(\theta, \phi)\rangle, \qquad (2)$$

where $u_{nl}(r)$ are the HO radial wave functions and C_{nl} the corresponding overlap coefficients,

$$C_{nl} \equiv \langle u_{nl}(r)Y_{lm}(\theta, \phi)|\varphi_j(\rho, z)e^{im\phi}\rangle. \qquad (3)$$

The angular momentum l in (2) is restricted to even or odd values according to the parity of the state.

The l component in k space for a single-particle orbital (j) is then given by

$$n_l^{(j)}(k) = \sum_{nn'} C_{nl}^* C_{n'l}\tilde{u}_{nl}^*(k)\tilde{u}_{n'l}(k), \qquad (4)$$

where $\tilde{u}_{nl}(k)$ is the Fourier transform of the corresponding wave function in r space, $u_{nl}(r)$, and the single-particle momentum distribution of the single-particle orbital is

$$n^{(j)}(k) = \sum_l n_l^{(j)}(k). \qquad (5)$$

The strength of the l-wave component in a given Kohn-Sham orbital is

$$n_l^{(j)} = \sum_n |C_{nl}|^2. \qquad (6)$$

These l-wave strengths allow us to analyze the relation between global deformation and the admixture of different l-waves for each orbital. Normalization of the single-particle orbitals implies that $\sum_l n_l^{(j)} = 1$.

3. Results

We will concentrate on those clusters containing 22, 24, and 42 atoms, which are clearly deformed [6–8, 15, 16], and compare with the predictions obtained for magic spherical clusters Na_{20} and Na_{40}, with filled electronic shells.

With the aim to analyze the effect of deformation on the single-particle distribution, we have compared the single-particle results of Na_{20} (spherical) with those of Na_{22} and

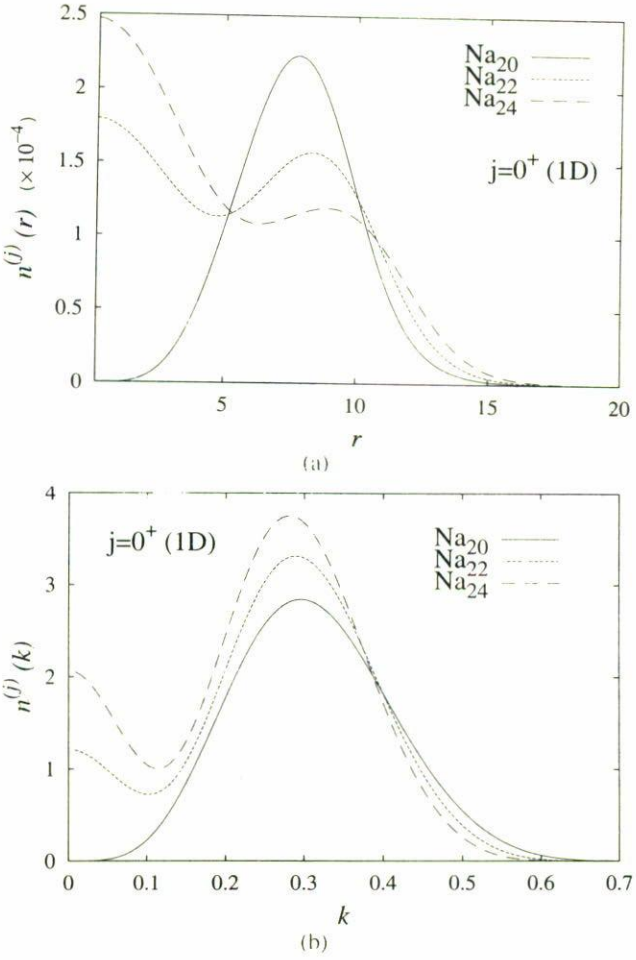

FIGURE 1. Single-particle density of the orbital 0^+ $(1D)$ for Na_{20}, Na_{22}, and Na_{24} in a) r and b) k space.

Na_{24}, as well as the results of Na_{40} (spherical) with those of Na_{42}, in r and in k spaces. The single-particle orbitals of the spheroidal deformed mean field (Na_{22}, Na_{24}, and Na_{42}) are characterized by the z-component of the angular momentum, m, and by the parity, π. Different states with the same m^π values are distinguished by their dominant spherical component (nl).

We have analyzed the electronic distribution in r and k spaces for each single-particle orbital. Each specific deformed orbital has its peculiarities, but for a given level $m^\pi(nl)$ we observe the same qualitative behavior in $Na_{20-22-24}$ as in Na_{40-42}. As an example we show in Figs. 1a and 1b the spherically averaged results for the orbital $0^+(1D)$ of $Na_{20-22-24}$ in r and k spaces. The main features concerning the differences between spherical and deformed clusters can be understood from the content of each l component (6) in the orbital. As it is shown in Table I, increasing deformation generates a depletion of the l dominant component and an enlargement of the components with $l' \neq l$. In particular the bump at the origin in Figs. 1a and 1b comes from the contribution of the S-waves, whose importance increases with deformation. The shift of the peak maximum

TABLE I. l-wave contribution to the single-particle momentum distribution of the orbital $0^+(1D)$ for Na_{20}, Na_{22}, and Na_{24}.

	$l=0$	$l=2$	$l=4$
Na_{20}	0	1	0
Na_{22}	0.121	0.866	0.009
Na_{24}	0.187	0.784	0.025

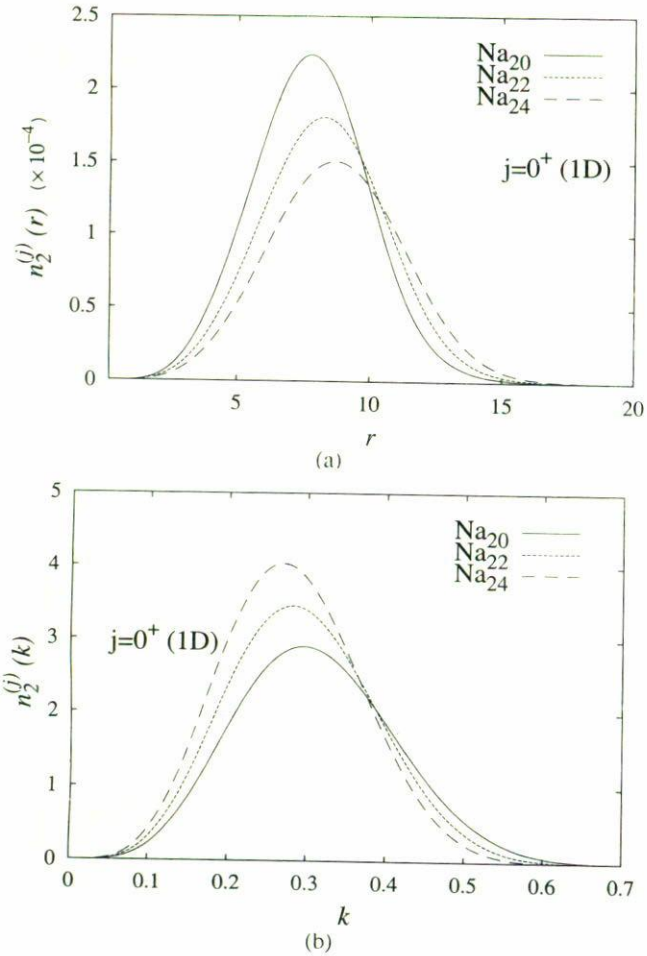

FIGURE 2. $l=2$ component of the orbital $0^+(1D)$ for Na_{20}, Na_{22}, and Na_{24} in a) r and b) k space .

shown in these figures (to the right in r space and to the left in k space) is due to the difference of the $l=2$ component between the spherical cluster and the deformed one (see Figs. 2a and 2b). Notice that deformation decreases the maximum value of the $l=2$ component in r space, whereas this maximum value increases in k space for the same component. For this orbital $0^+(1D)$ the increasing of the deformation tends to increase $n(k)$ at small k values and to reduce its tail at high momentum, conversely to what happens in r space where tails increase with deformation. This feature can be understood heuristically from the Heisenberg uncertainty principle, $\sqrt{\langle r^2\rangle}\,\sqrt{\langle k^2\rangle} \sim 1$.

TABLE II. l-wave contribution to the single-particle momentum distribution of the orbital $0^+(2S)$ for Na_{40} and Na_{42}.

	$l=0$	$l=2$	$l=4$
Na_{40}	1	0	0
Na_{42}	0.755	0.232	0.012

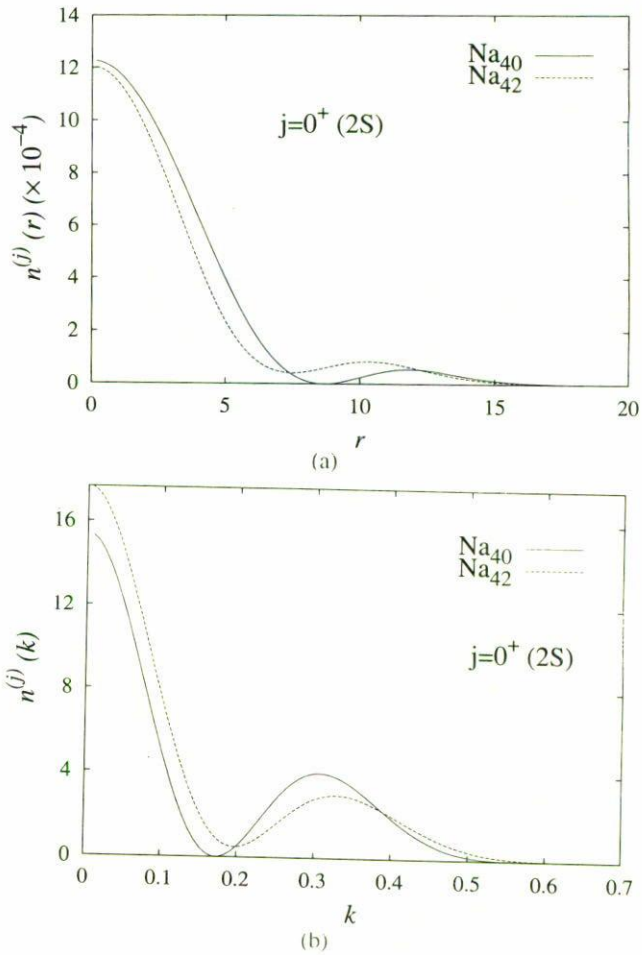

FIGURE 3. Single-particle radial density of the orbital $0^+(2S)$ for Na_{40}, and Na_{42} in a) r and b) k space.

As another example of deformation effects on the single-particle distributions, Figs. 3a and 3b and Table II show the pertinent analysis for the $0^+(2S)$ orbital of Na_{40-42} in r and k space. In this case the different value at the origin comes from the difference in the $l=0$ projected component between the spherical (Na_{40}) and the deformed cluster (Na_{42}). For this orbital, and contrary to what we have discussed about the orbital $0^+(1D)$, an increasing deformation gives larger tails in momentum space and, consequently, reduces the radial density at large distances in r space. In Na_{42} the admixture between $l=0$ and $l=2$ projected components (Table II) is greater than for Na_{22} and Na_{24} (see Table I) according to the larger value of the global deformation parameter in r space [16].

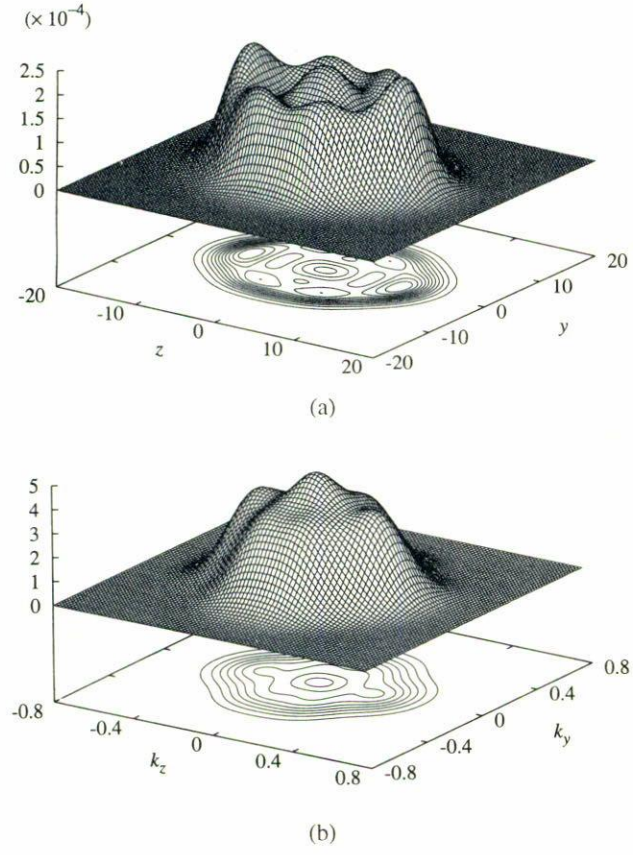

FIGURE 4. Overall a) density in r space in the plane $x = 0$ and b) momentum distribution in the plane $k_x = 0$ for Na_{22} normalized to unity.

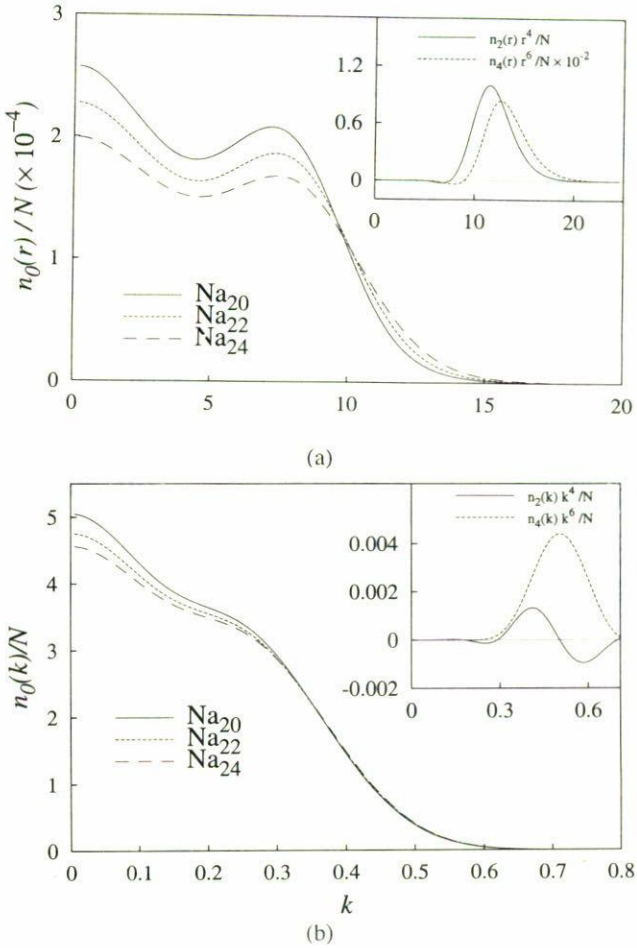

FIGURE 5. Monopole component of a) the electronic density in r space and b) the global momentum distribution for Na_{20}, Na_{22}, and Na_{24}. a) $n_2(r)\, r^4/N$ and $n_4(r)\, r^6/N \times 10^{-2}$ *vs.* r and b) $(n_2(k)\, k^4/N)$ and $(n_4(k)\, k^6/N)$ *vs.* k for Na_{22} are shown in the inset.

Thus, individual shells show important differences depending on the deformation of the cluster both in r space and in k space. This is in contrast with the behavior found for overall momentum distributions

$$n(\vec{k}) = \sum_{\lambda} n_\lambda(k) P_\lambda(\Omega_k). \tag{7}$$

The latter together with the overall density in r space are shown for Na_{22} in Figs. 4. $n(\vec{r})$ is clearly deformed but $n(\vec{k})$ shows only a small deformation that mainly comes from the contribution of the $\lambda = 4$ polar component. Each λ-polar component $n_\lambda(k)$ allows to obtain a λ-polar momentum as a measure of deformation

$$Q_k^\lambda = \frac{1}{N}\left(\frac{2\pi}{2\lambda+1}\right)^{1/2} \int k^{j+2} n_\lambda(k)\, dk. \tag{8}$$

Analogously, $n_\lambda(r)$ and Q_r^λ are defined in r space. As it is clearly shown in Figs. 5a and 5b, $n_2(r)$ leads a strong peak at the cluster surface that integrates to give a quite sizeable quadrupole moment, while in k space $n_2(k)$ has a small oscillation that integrates to zero. More details can be found in Tables I and II of Ref. 15. The $\lambda = 4$ polar component gives the main contribution at the surface of r space and is responsible for the small deformation in k space. Nevertheless, due to its small value the main properties of the global momentum distribution can be obtained from its monopole component $n_0(k)$, and can be understood on the basis of the Slater approach used for spherical clusters [15]. As an example, Figs. 5a and 5b also show the monopole components of the electronic distributions in r and k spaces for Na_{20}, Na_{22}, and Na_{24}. In both figures, the three profiles are similar and one verifies that shell effects diminish with deformation. According to the Slater approach [15] the increase of the surface thickness in r space implies the increase of $n_0(k)$ at small k values. Nevertheless this effect is compensated by the different values of the number of particles N in the normalization constant of $Na_{20,22,24}$.

4. Conclusions

We have compared the main properties of spheroidal deformed clusters in r and k spaces using the Kohn-Sham formalism. In spite of the fact that the global electronic distribution for clusters with unfilled electronic shells is clearly

deformed in r space, in k space the global momentum distribution is basically reproduced by its monopole component, and its main features can be understood from the Slater approach as in the case of spherical clusters.

In k space deformation effects can be mostly seen in the single-particle distributions. There is not a general rule to characterize the deformation effects in single-particle orbitals since they are specific to each orbital. The differences between spherical and deformed orbitals are signatures of the admixtures of different l-components caused by the deformation of the mean field, and are present both in r and in k spaces. The qualitative behavior in r and k spaces can be related using the Heisenberg uncertainty principle.

Acknowledgments

This work has been supported by DGICYT (Spain), Grant Nos. PB95-0492 and PB95-0123.

1. W.A. de Heer, *Rev. Mod. Phys.* **65** (1993) 611.
2. M. Brack, *Rev. Mod. Phys.* **65** (1993) 677, and references therein.
3. J. Borggreen *et al.*, *Phys. Rev. B* **48** (1993) 17507.
4. P. Meibon *et al.*, *Z. Phys. D* **40** (1997) 258.
5. Th. Hirschman, M. Brack, and P.G. Reinhard, *Z. Phys. D* **40** (1997) 254.
6. K. Clemenger, *Phys. Rev. B* **32** (1985) 1359.
7. S.M. Reiman, M. Brack, and K. Hansen, *Z. Phys. D* **28** (1993) 235.
8. W. Ekardt and Z. Penzar, *Phys. Rev. B* **38** (1988) 4273; *Phys. Rev. B* **43** (1991) 1322; Z. Penzar and W. Ekardt, *Z. Phys. D* **17** (1990) 69.
9. P. Meier, M. Brack, and S.C. Creagh, *Z. Phys. D* **41** (1997) 281.
10. M. Vos, Z. Fang, S. Canney, A. Kheifets, and I.E. McCarthy, *Phys. Rev B* **56** (1997) 963.
11. M. Vos *et al.*, *Phys. Rev. B* **56** (1997) 1309.
12. D.A. Peek and R.O. Simmons, *J. Chem. Phys.* **94** (1991) 3169.
13. G. Ortiz and P. Ballone, *Phys. Rev. B* **50** (1994) 1391.
14. A. Bulgac and J.M. Tompson, *Phys. Lett. B* **383** (1996) 127.
15. A. Rigo *et al.*, *Z. Phys. D* **40** (1997) 294.
16. A. Rigo *et al.*, *Phys. Rev. B* **57** (1998) 11943.
17. G.B. West, *Phys. Rep.* **18** (1975) 263; J.J. Kelly, *Adv. Nucl. Phys.* **23** (1996) 75.